

# Comparison between a Crank-drive Reciprocating Compressor and a Novel Oil-free Linear Compressor

Kun Liang\*, Richard Stone, William Hancock, Mike Dadd, Paul Bailey

Department of Engineering Science, University of Oxford, Oxford, UK, OX1 3PJ

\* *Corresponding author:* Department of Engineering Science, University of Oxford, Oxford OX1 3PJ, UK. Email address: kun.liang@eng.ox.ac.uk (K. Liang)

## Abstract

Reciprocating compressors, driven by induction motors through a crank mechanism, have been commercially used over many years for refrigeration. An oil-free linear compressor driven by a moving magnet motor was designed, for a refrigeration system with a compact heat exchanger. Measurements using nitrogen are reported here to compare the motor performance and overall efficiencies of the two types of compressor with comparable design parameters. The experimental results show that the moving magnet linear motor has a much higher motor efficiency than the conventional induction motor, particularly at low power inputs. However, with a much smaller clearance volume (approaching zero), the crank-drive compressor demonstrates a higher volumetric efficiency based on the swept volume, that is approximately 20% higher than the linear compressor when operated at its maximum stroke (13 mm). It is anticipated that with a revised design, the overall performance of the linear compressor could be enhanced further.

Keywords: Linear motor, induction motor, crank-drive, oil-free linear compressor, efficiencies

## NOMENCLATURE

$A$	area ( $\text{mm}^2$ )
BLDC	brushless direct-current
$c$	radical clearance ( $\mu\text{m}$ )
$C$	capacitance (F)
$CL$	clearance
CSIR	capacitor start induction run
DC	direct current
$f$	frequency (Hz)
$F$	force (N)
FE	finite element
FFT	fast Fourier transform
HDAQ	high-speed data acquisition
$i$	current (A)
$k$	stiffness ( $\text{kN m}^{-1}$ )
$L$	inductance (H) or length (mm)
LDAQ	low-speed data acquisition
LVDT	linear variable differential transformer
$m$	moving mass (kg)
$\dot{m}$	mass flow rate ( $\text{g s}^{-1}$ )
$n$	polytropic index
$P$	pressure (bar)
$R$	resistance ( $\Omega$ ) or specific gas constant ( $\text{J kg}^{-1} \text{K}^{-1}$ )
RSIR	resistive start induction run
$T$	temperature (K)
TC	thermocouple
$V$	volume ( $\text{mm}^3$ ) or voltage (V)
VF	vector field
$\dot{W}$	power (W)
$x$	displacement (mm)

## Greek

$\gamma$	heat capacity ratio
$\eta$	efficiency
$\beta$	damping coefficient

## Subscripts

adb	adiabatic
b	body
c	cylinder
dis	discharge
e	experimental
EMF	electromagnetic force
g	gas
in	input
m	motor/mechanical
t	thermodynamic
o	overall
S	swept
suc	suction
V	volumetric

## **1. Introduction**

The piston in a conventional reciprocating compressor commonly used for refrigeration is driven by an induction motor through a crank mechanism, providing a reciprocating motion to compress the gas. The presence of the crank and bearings reduces the mechanical efficiency significantly. Furthermore, oil lubrication in crank-drive compressors narrows both the choice of refrigerants and their operating temperature range. Oil films inside the heat exchangers lower the heat transfer coefficients, especially in compact heat exchangers.

These problems can be mostly solved in a linear compressor, in which the piston is directly coupled to a linear oscillating motor. The spring suspension system ensures that the piston moves linearly, and there is a small radial clearance ( $\sim 10\text{ }\mu\text{m}$ ) between the piston and cylinder to provide a so-called ‘clearance seal’. So there is no physical seal, but there will be a leakage loss, and this is discussed later with Fig. 13. The elimination of the crank makes oil-free operation possible in linear compressors, which is one of the main advantages. Linear compressors operate at resonance in order to minimise the drive current, allowing higher motor efficiency and a reduction in the size of the motor as well. Bansal et al. (2011) reviewed the advantages of linear compressor technologies over traditional crank-drive reciprocating compressors for domestic applications and concluded that linear compressors offer higher efficiency and a more promising alternative to control the refrigeration capacity.

Since the 1970s, there have been some developments in this area. Bradshaw et al. (2011) have reported both the early and some more recent linear compressor developments. Bailey et al. (2010) reviewed the three generations of moving coil linear compressors designed at the University of Oxford for space application (Bradshaw et al., 1986; Davey, 1990; Bailey et al., 2001). Liang et al. (2013) have reported on the recent development of a moving magnet linear compressor, other examples of which can be found in Beale and Scheck (1986), Yarr and Corey (1995), Nasar and Boldea (1997) and Lilie (2008).

Bradshaw et al. (2012) utilized the compressor model in Bradshaw et al. (2011) to compare the energy recovery characteristics of a linear compressor to those of a crank-drive reciprocating compressor and demonstrated that the linear compressor could operate more efficiently over a wider range of dead (clearance) volumes than the crank-drive compressor. Ku et al. (2010) measured the performances of a moving magnet linear compressor (of Sunpower design) and a brushless direct-current (BLDC) reciprocating compressor, and concluded that the linear compressor had a power consumption reduction of about 10% as compared with the BLDC reciprocating compressor.

A new design of low-cost moving magnet type linear compressor for use with compact refrigeration heat exchangers was completed at the University of Oxford in 2009, based on successful oil-free technology used in space refrigeration applications. A prototype of this new linear compressor using NdFeB magnets was built for experimental investigations. A small commercial crank-drive reciprocating compressor (hereafter referred to as ‘crank-drive compressor’) has been experimentally evaluated so as to be compared with the linear compressor using nitrogen as working fluid. This provides preliminary performance data with single phase (gas) operation. This work focuses on the performances of the compressors themselves, and refrigeration measurements will be the subject of future work.

## **2. Compressor Specifications**

### **2.1 Crank-drive Compressor**

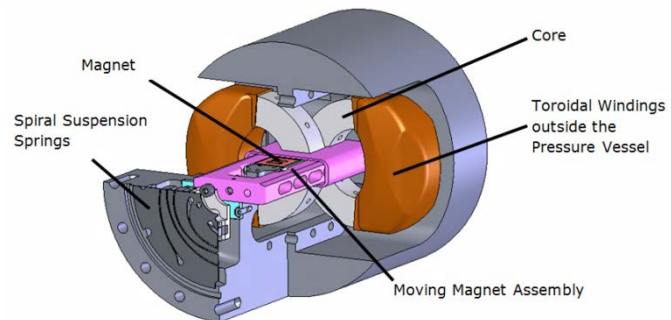
The crank-drive compressor for comparison is a commercial compressor for household refrigeration, which employs a single-phase induction motor to drive the piston, with the specification given in Table 1.

**Table 1** Specification of the crank-drive compressor

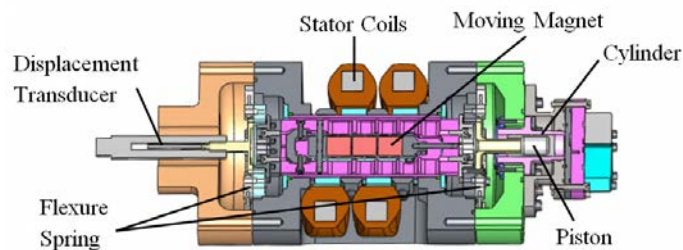
Motor type	RSIR/CSIR
Resistance in main winding ( $\Omega$ )	12.6
Resistance in start winding ( $\Omega$ )	12.4
Stroke (mm)	18
Piston diameter (mm)	21
Piston length (mm)	20
Clearance volume (mm <sup>3</sup> )	125

## 2.2 Linear Compressor

Fig. 1 shows the key components of the moving magnet motor, including the linear suspension system (two sets of spiral springs), the static assembly (4 magnetic circuits consisting of coils wound on laminated and slotted cores to form an air gap) and the moving assembly (3 rectangular magnets in a line occupying the air gap) attached to the piston. When an alternating current is supplied to the cores, an alternating axial force will be induced in the moving magnet assembly, making the piston reciprocate at the same frequency. Further details of the compressor have been reported by Bailey et al. (2009).



(a) Moving magnet motor design



(b) Cross section of the linear compressor and motor

**Fig. 1** Design of the 100W Oxford moving magnet compressor

Table 2 gives the design specification of the moving magnet compressor, which uses two identical compressor halves mounted back-to-back in-line to minimise vibration. The maximum displacement is 3970 mm<sup>3</sup>.

**Table 2** Specification of each linear compressor half

Total mass of magnet/piston (kg)	0.66
Piston diameter (mm)	18.99
Total series <sup>1</sup> resistance of coils ( $\Omega$ )	14
Peak shaft force (N)	84
Peak current at peak force (A)	1.29
Flexure stiffness (Total) ( $\text{kN m}^{-1}$ )	17
Maximum stroke (mm)	14

<sup>1</sup>The four motor coils were connected with two coils in series then each pair in parallel to give a resistance of  $\sim 3.5 \Omega$  for each compressor half.

### 3. Compressor Tests using Nitrogen

#### 3.1 Crank-drive Compressor Test Rig

Fig. 2 shows the experimental apparatus for the crank-drive compressor working with nitrogen. Two pressure transducers and K type thermocouples are used to measure the pressure and temperature of the suction and discharge lines. The pressure transducers were calibrated by using a dead weight tester, which applied a test pressure to the transducer by loading a piston of known area with standard weights. As the original thermocouples only produce a few mV output, an amplifier was designed. The thermocouples were calibrated by comparing their output voltages to known reference temperatures provided by mercury in glass thermometer with 0.2 K resolution. A positive displacement volume flow meter is employed to determine the mass flow rate when it exceeds 0.5 g/s, which is beyond the range of the mass flow meter in the inlet line. The volume flow rate was converted to a mass flow rate since the temperature and pressure were also measured. The MKS mass flow meter was calibrated by using a positive displacement volume flow meter in the inlet line and a voltmeter at the output of the mass flow meter.

An oil separator removes the compressor lubricant from the compressed gas so that the volume flow meter is not affected or possibly damaged. The suction pressure was manually controlled by a pressure regulator and the discharge pressure was set by a needle valve. The power input to the compressor was measured by a power meter. An eight channel Fylde Micro-analog 2 USB DAQ card was used for both the low-speed DAQ system (LDAQ) and high-speed DAQ system (HDAQ).

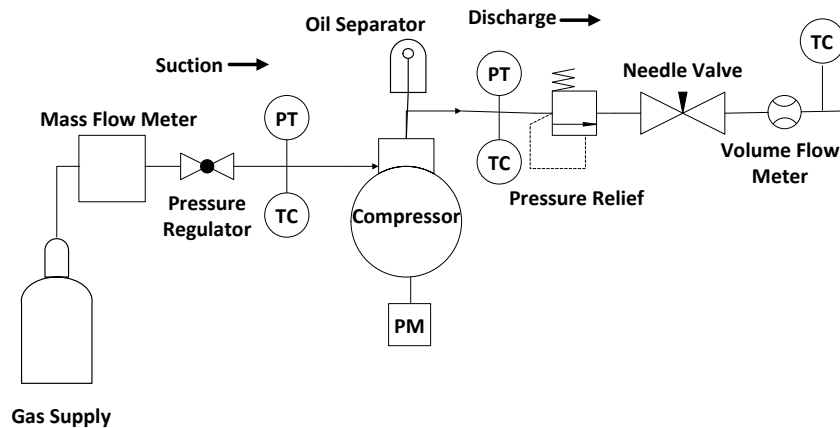


**Fig. 2** Crank-drive compressor test rig diagram using nitrogen (PT: Pressure Transducer, TC: Thermocouple, PM: Power Meter)

After completion of the crank-drive compressor tests, the compressor was dismantled so that the induction motor could be tested. The induction motor was connected to a motor test rig (Leroy Somer

test bed, with a tachometer, a dynamometer and a Modmeca 3 dynamometer control box) to be characterized. This allowed the speed and torque to be measured, and hence the calculation of the motor output power. Varying the torque changed the power input to the induction motor so that the motor efficiency could be determined.

### 3.2 Linear Compressor Test Rig

The test rig for the linear compressor is significantly different from the crank-drive compressor test rig because it needs to be completely oil-free. The linear compressor test loop is shown in Fig. 3. It is designed for refrigerant tests and is also suitable for measurements using gas. Displacements of the pistons are measured by two Schaevitz LVDTs (not shown in Fig. 3). Both LVDTs were calibrated to obtain the sensitivity factor and the phase shift response with operating frequency. The main flow valve (needle valve) controls the pressure ratio and the bleed valve adjusts pressure in the compressor body so as to maintain an appropriate mean position of the piston. Both mass flow rates in main and bleed flow loops are measured through mass flow meters (Hastings HFM 201 for the main flow and Tylan 360 for the bleed flow). Calibration of the two mass flow meters for nitrogen was done by Teledyne Instruments and Chell Instruments respectively.

Pressures and temperatures of the compressor body, the discharge line and the suction line were all measured by pressure transducers and K-type thermocouples, which were calibrated using similar methods to those discussed in Section 3.1. An interface box was built to provide the pressure transducers with power and provide amplifiers for the thermocouples. The currents going into the two compressor halves were measured by a current transducer with two channels. A power meter displayed the electrical power input and RMS values of current and voltage. Two NI 6251 DAQ cards (16 analog channel,  $1.25 \text{ MS s}^{-1}$ ) were used for both low-speed DAQ sampling and high-speed DAQ sampling.

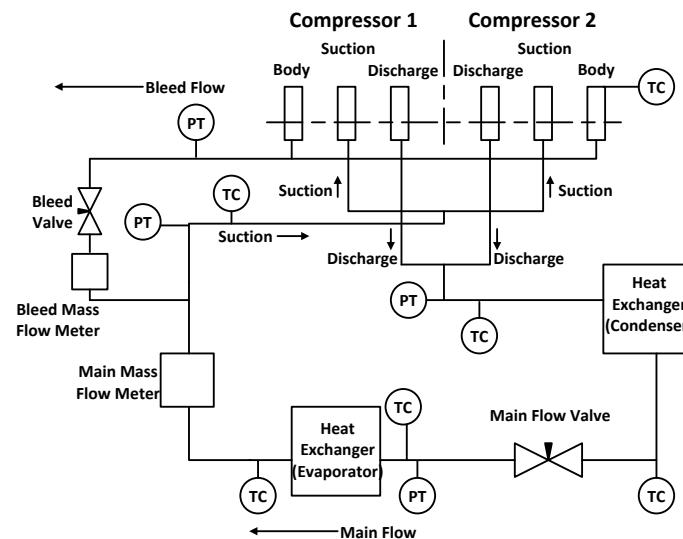


**Fig. 3** Overall experimental apparatus for the linear compressor (PT: Pressure Transducer, TC: Thermocouple)

The operating frequency was manually adjusted using a signal generator so that the resonance can be identified at which the power was a minimum for the specified stroke and applied to the linear motor. The piston stroke (Peak-to-Peak value from an oscilloscope) was set by a voltage amplitude control followed by a power amplifier which finally amplified the analogue signal to drive the compressor. A capacitance box was employed to permit correction of the power factor in response to different

resonant frequencies. Fig. 4 illustrates the equivalent electrical circuit of the linear motor. The voltage required can be given as:

$$V = V_{\text{EMF}} + L \frac{di}{dt} + iR + \frac{1}{C} \int i dt \quad (1)$$

where  $V_{\text{EMF}}$  is the electromotive force and  $V_{\text{EMF}} = \kappa \dot{x}$  ( $\kappa$  is the motor force constant).

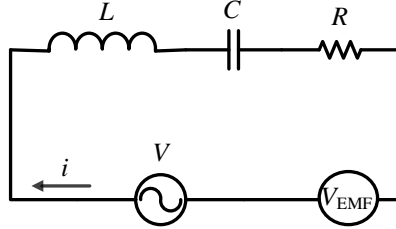


**Fig. 4** Simplified model for the circuit of the linear motor (EMF: electromotive force)

Therefore, the capacitance  $C$  required to reduce the voltage can be inferred from the resonant frequency equation of the LC circuit as

$$C = \frac{1}{4\pi^2 f^2 L} \quad (2)$$

where  $f$  is the resonant frequency and the inductance  $L$  is 0.141 H.

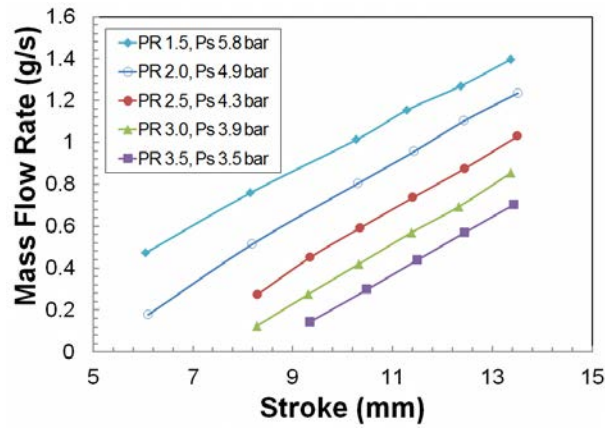
### 3.3 Test Conditions

Table 3 lists the test conditions using nitrogen for the two compressors. Experiments on the linear compressor were conducted for variable strokes at different pressure ratios. Prior to the measurements, the linear compressor was filled to 7 bar absolute as a ‘fill pressure’. The suction pressure slightly changes with stroke at each fixed pressure ratio. However, the mass flow rate changes almost linearly with stroke for each pressure ratio. This is shown in Fig. 5.

In order to obtain comparable data with the linear compressor, the crank-drive compressor was tested with variable suction pressures at different pressure ratios. A series of tests was undertaken with the same suction pressure as the linear compressor operating at 13 mm stroke (maximum stroke) at each pressure ratio. In addition, for each fixed pressure ratio, the suction pressure was varied in the crank-drive compressor to maintain a similar mass flow rate to the linear compressor.

**Table 3** Test conditions for the two compressors

Gas	Crank-drive compressor	Linear compressor
	nitrogen	
Drive frequency (Hz)	50 (fixed)	28.5 – 40.5
Suction pressure (bar)	1.2 -5.0	3.6 – 5.8
Pressure ratio	1.4 – 3.8	1.5, 2.0, 2.5, 3.0, 3.5
Stroke (mm)	18 (fixed)	6, 8, 10, 11, 12, 13
Mass flow rate (gs <sup>-1</sup> )	0.25 – 1.51	0.12 – 1.39
HDAQ sampling rate (kS s <sup>-1</sup> )	5	5
HDAQ sampling number	2000	5000
LDAQ sampling rate (kS s <sup>-1</sup> )	1	1



**Fig. 5** Mass flow rate as a function of stroke at different pressure ratios (PR) and suction pressures (Ps) for the linear compressor

### 3.4 Linear Motor/Compressor Analysis

For the linear compressor, the resonant frequency of the moving assembly is determined by the moving mass, and the combined stiffness of the mechanical (flexure) spring and the gas spring. Fig. 6 shows the measured resonant frequency changing with stroke and pressure ratio for a fill pressure of 7.0 bar. It can be seen that a higher pressure ratio produces a higher resonant frequency due to larger induced gas spring stiffness. It is also noticeable that for a set pressure ratio the resonant frequency decreases as the stroke increases. For a variation in stroke from 8 to 13 mm, the resonant frequency varies by about 10%. For a fixed pressure ratio, increasing the stroke means that the valves will be open for a greater fraction of the cycle, so that the ‘effective stiffness’ associated with compressing the gas is reduced. For the design point (stroke of 13 mm and pressure ratio of 3.0), the resonant frequency is 36.5 Hz.

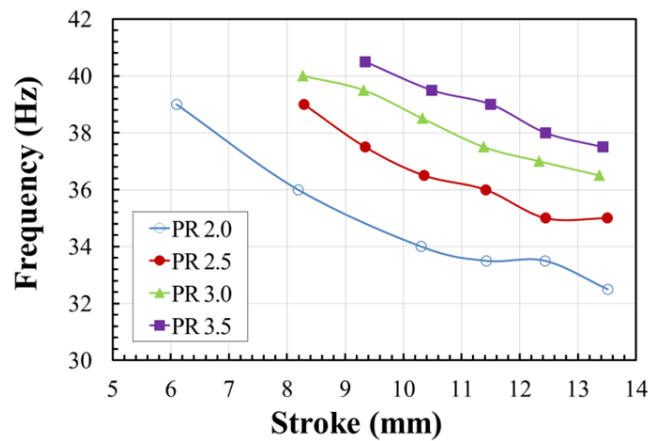


**Fig. 6** Resonant frequency variation with stroke at different pressure ratios (PRs) when the linear compressor was initially filled to 7 bar

For the motor performance comparison, the linear motor characteristic was calibrated ahead of the measurements. A comparison of the force/current constants between the Vector Field (VF) Finite Element (FE) model and the experimental calibration for two compressor halves (1 and 2) is shown in Fig. 7. The simulation tool is the TOSCA analysis package, a module in Vector Field’s OPERA-3D software. The motor force characteristics calibration provided a 3D map (force-current-displacement) so that with the measured current and displacement signals, the force can be interpolated from the map, instead of using a force/current constant.



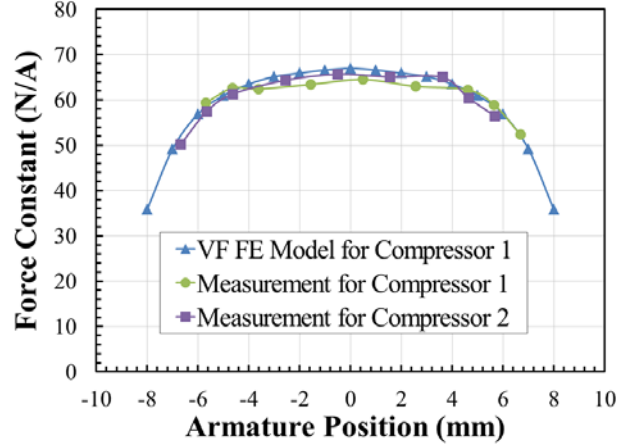


**Fig. 7** Linear motor force constant variation with armature position from measurements and Vector Field (VF) Finite Element (FE) model

This knowledge along with the moving mass and spring stiffness enables the equation of motion to be solved, so that the absolute cylinder pressure can be derived. The performance of the free-piston linear compressor has been previously modelled with a one-dimension mathematical model by Davies et al. (2010), so as to help with design optimization and the identification of key parameters affecting system transients. A schematic of the compressor model including the key parameters is shown in Fig. 8. The reciprocating piston is directly attached to the linear motor. The piston assembly consists of a free piston, a shaft and a moving magnet assembly enclosed in a rectangular tube.

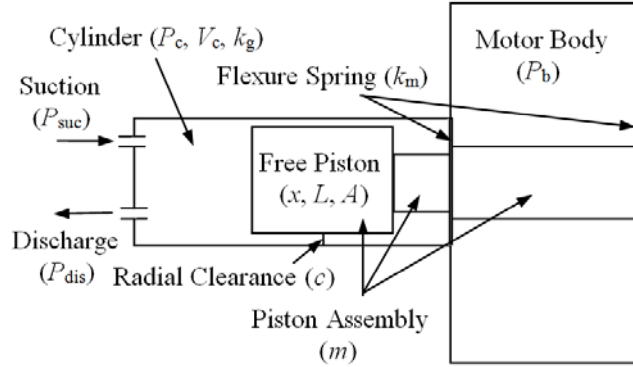


**Fig. 8** Schematic of the linear compressor model showing key parameters (adapted from Davies et al. [16])

The cylinder gas pressure force can be inferred from the piston dynamics as

$$F_{\text{cylinder}} = F_{\text{motor}} - F_{\text{piston}} - F_{\text{spring}} - F_{\text{damping}} + F_{\text{body}} \quad (3)$$

This can be expanded further to give

$$P_c = (F_{\text{motor}} - m\ddot{x} - k_m x - \beta\dot{x})/A + P_b \quad (4)$$

where  $\beta$  is the damping coefficient and  $m$  is the moving mass given in Table 2.

Fig. 9 shows a computed  $P$ - $V$  diagram for the linear compressor operating at a stroke of 13 mm and a pressure ratio of 2.5 in which the suction and discharge pressures from measurements have also been plotted. It is worth emphasising that the suction and delivery pressures were not used in deriving the cylinder pressure, so these provide useful corroboration of the cylinder pressure.

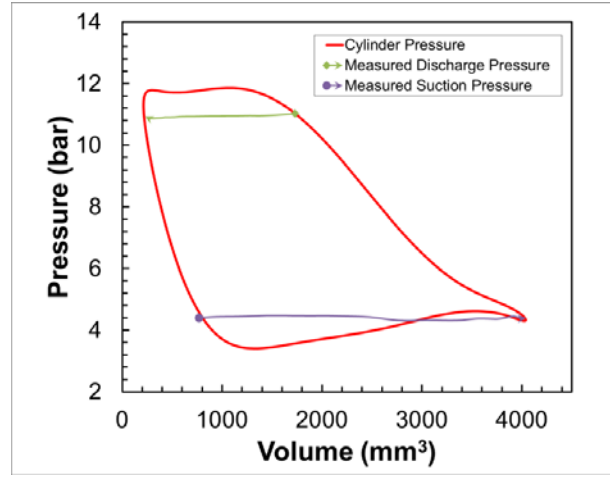


**Fig. 9** Derived  $P$ - $V$  diagram for the linear compressor operating at a stroke of 13 mm and a pressure ratio of 2.5

### 3.5 Data Reduction

For an adiabatic process with an ideal gas, the theoretical power can be calculated according to

$$\dot{W}_{adb} = \frac{\gamma}{\gamma-1} \dot{m} R_g T_{suc} \left[ \left( \frac{P_{dis}}{P_{suc}} \right)^{\frac{\gamma-1}{\gamma}} - 1 \right] \quad (5)$$

The motor efficiency (or electrical efficiency) is defined as the motor output power over the power input

$$\eta_m = \frac{P_m}{P_{in}} \quad (6)$$

The thermodynamic efficiency is defined as

$$\eta_{t,adb} = \frac{\dot{W}_{adb}}{P_m} \quad (7)$$

Hence, the overall efficiency will be

$$\eta_{o,adb} = \eta_{t,adb} \eta_m = \frac{\dot{W}_{adb}}{P_{in}} \quad (8)$$

The volumetric efficiency (experimental) can be computed from the measured mass flow rate, operating frequency and swept volume as

$$\eta_{v,e} = \frac{\dot{m} R_g T_{suc}}{V_s f P_{suc}} \quad (9)$$

## 4. Motor Performance

### 4.1 Motor Efficiency

Fig. 10 shows the motor efficiency variation with the motor output power for the two types of compressor. The induction motor data is from the tests with the dynamometer. The linear compressor was operated at its resonant frequency with different strokes at a pressure ratio of 3.0 (design point) for comparison. In general, the linear motor efficiency is higher than the induction motor, particularly

at lower motor output powers (82% at a motor output of 40 W compared with 23% for the induction motor). In contrast, the linear motor efficiency decreases with motor output power while the induction motor efficiency increases. In the linear motor, when the supplied current increases, the copper loss ( $I^2R$ ) rises more rapidly than the shaft force does, resulting in a decreasing efficiency. In contrast, the induction motor requires power to magnetize the core so that the efficiency is very low at low power inputs, but rises rapidly as the power output increases, so its efficiency increases. As the current increases in the induction motor, the torque output increases more quickly than the copper loss plus the core loss (which is approximately constant).

The maximum induction motor efficiency is approximately 60% at an electrical power input of 249 W. In contrast, the minimum linear motor efficiency is about 72% when the compressor operated at a stroke of 13 mm and a pressure ratio of 3.0 with a power output of 126 W. This comparison indicates that the linear motor has an efficiency advantage over the conventional induction motor.

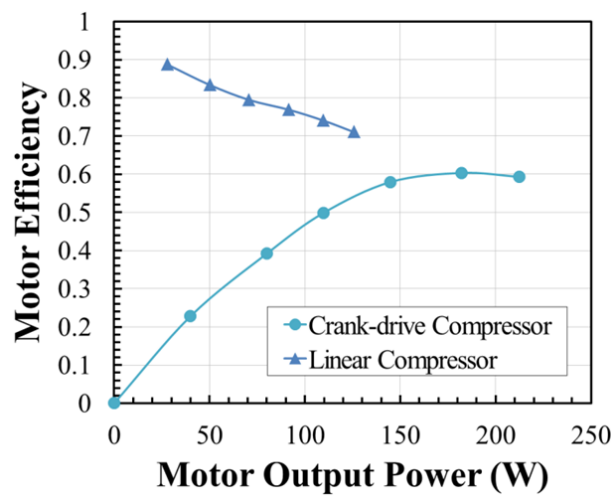


**Fig. 10** Motor efficiency comparison between the crank-drive compressor and the linear compressor (when operating at a pressure ratio of 3.0)

## 4.2 Motor Losses

Losses in the linear motor include the copper losses, hysteresis loss and the eddy current losses. In addition to reducing its performance, they generate undesired heat and noise. The hysteresis loss and eddy current loss are normally given in total as a core loss by the manufacturer of the core material, as a function of peak magnetic flux density and frequency. However, there were two additional eddy current losses occurring in the compressor pressure containment tube and the aluminium body (estimated as 5 W and 10 W for the design point at 36.5 Hz) in this prototype compressor. These additional eddy current losses could be significantly reduced with a revised design, by using materials with a lower electrical conductivity or thinner sections, so that the motor efficiency is predicted to increase to approximately 86%.

In the induction motor, the parasitic losses are the core loss, copper losses and other minor losses. The core loss is the energy required to magnetize the core. The copper losses ( $I^2R$ ) exist in both stator (main winding) and rotor (conductive bars). The core loss in the induction motor can be inferred from the vacuum tests assuming that the leakage and friction effects are small enough to be ignored. By using an FFT on the discharge pressure signal (from the HDAQ), the fundamental frequency (the rotor mechanical speed) was found (48.83 Hz) to give a slip of 2.3%.

Table 4 gives the comparison of losses between the linear motor and the induction motor for the same motor output power. It can be seen that the core loss in the induction motor is about half the total loss (94.4 W) while the total linear motor loss is only 47.3 W. Therefore, to provide a similar motor power to compress the gas, the linear motor requires much less electrical power.

**Table 4** Losses in the two types of motor at an output power of 120 W

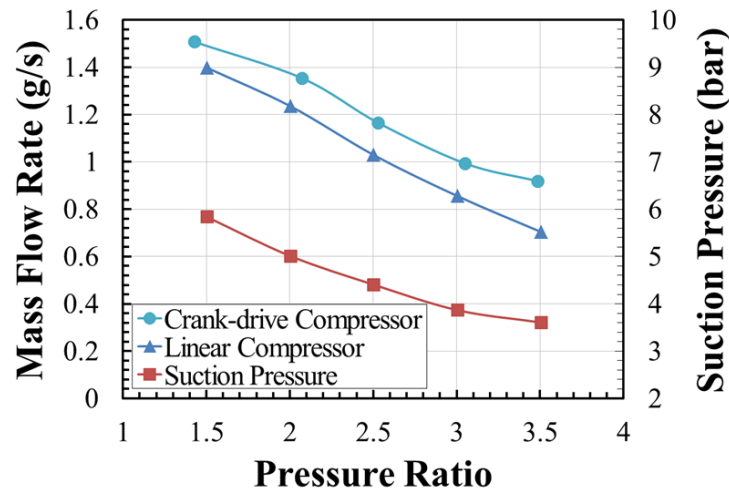
	Linear motor	Induction motor
Total power input (W)	167	214
Copper loss (W)	29	25
Core loss (W)	3	47
Additional losses (W)	15	22
Motor output power (W)	120	

## 5. Compressor Efficiency

### 5.1 Overall Efficiency

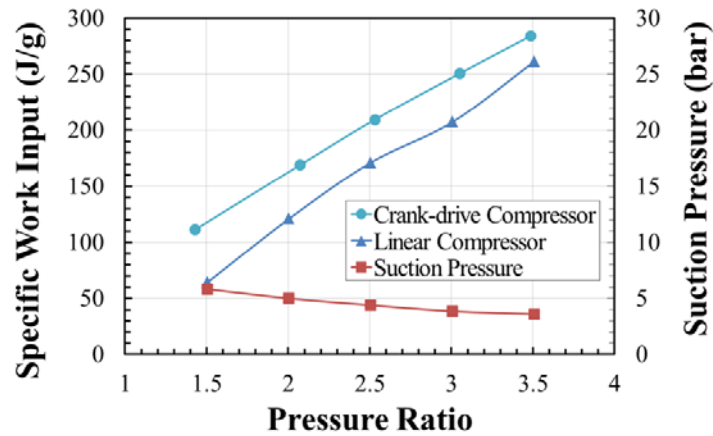
The linear compressor measurements were conducted first to give values of the suction pressure with a 13 mm stroke for each pressure ratio. The suction pressures in the crank-drive compressor test were regulated to be the same for each pressure ratio.

Fig. 11 gives the mass flow rate and the suction pressure for two compressors against the pressure ratio. It is seen that the mass flow rate reduces as the pressure ratio rises in both compressors when the crank-drive compressor operates at a fixed speed and the linear compressor runs at a fixed stroke. The average difference between two compressors for each pressure ratio is  $0.14 \text{ g s}^{-1}$ . With a pressure ratio of 2.0 the resonant frequency was 32.5 Hz for a stroke of 13 mm, but with the pressure ratio of 3.0 the resonant frequency increased to 36.5 Hz for the same stroke because of the gas-spring effect.



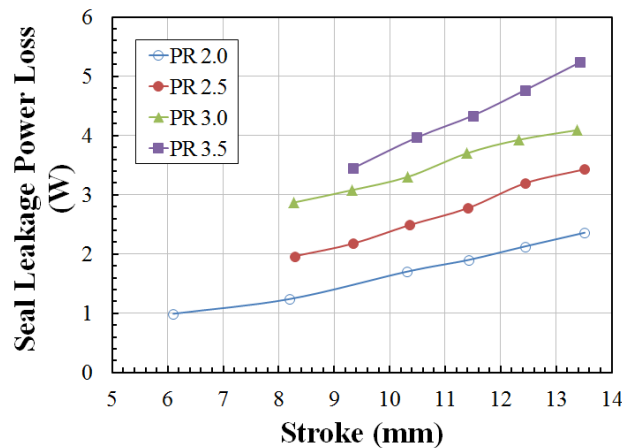
**Fig. 11** Mass flow rate measured against pressure ratio; the linear compressor was operated with a 13 mm stroke

Fig. 12 shows the specific work (the ratio of the electrical power to the mass flow rate) into the two compressors as a function of the pressure ratio. The two curves follow a very similar trend. Due to its lower motor efficiency, the crank-drive compressor requires about  $50 \text{ J g}^{-1}$  more work than the linear compressor at each pressure ratio.



**Fig. 12** Specific work input for varying pressure ratio in the two compressors; the linear compressor was operated with a 13 mm stroke

For the linear compressor, previous tests on the discharge and suction reed valves show that there is hardly any leakage across the valves when they are closed for the compression or expansion process. However, there is a significant mass flow leakage across the clearance seal. The clearance seal leakage in the linear compressor has been modelled in Liang et al. (2013). Based on this model with experimental data, the power loss caused by the seal leakage is calculated and given in Fig. 13, as a function of the stroke at different pressure ratios. It can be seen that the seal loss increases with increasing stroke almost linearly and the gradient increases as the pressure ratio rises. The maximum seal loss is about 5.2 W, approximately 4% of the motor output power. For the crank-drive compressor, the leak tests on the valves indicated that leakage across the valves and piston are not significant.



**Fig. 13** Seal leakage power loss against stroke at different pressure ratios in the linear compressor

Mechanical friction in the linear compressor is assumed to be very small. For the crank-drive compressor, however, there are significant mechanical friction losses resulting from the bearings and the friction of the piston sliding in the cylinder.

Fig. 14 compares the thermodynamic efficiency and overall efficiency for the two compressors based on the ideal adiabatic work. The thermodynamic efficiency does not change very much for either compressor over the range of pressure ratios (on average 76% for the linear compressor and 72% for the crank-drive compressor). The linear compressor has a slightly higher thermodynamic efficiency at each pressure ratio than the crank-drive compressor, indicating that the pressure drop loss across the valves plus the clearance seal loss in the linear compressor is lower than the frictional loss plus

pressure drop loss in the crank-drive compressor. As the friction loss is only a small amount of the motor output power in the crank-drive compressor and the seal loss represents about 2-4% of the motor output power in the linear compressor, it can be argued that the pressure drop loss across the valves is very similar in the two compressors.

The overall adiabatic efficiency of the crank-drive compressor increases with the pressure ratio due to the increase of its motor efficiency as the power increases. In contrast, the linear compressor demonstrates a decreasing trend of overall efficiency against the pressure ratio, because the motor efficiency in the linear compressor slightly decreases with the increasing pressure ratio at the 13 mm stroke. However, the overall efficiency of the linear compressor is generally higher than the crank-drive compressor. The highest overall efficiency is about 60% in the linear compressor and 45% in the crank-drive compressor. Under a typical operation condition (pressure ratio of 3.0), the overall adiabatic efficiency in the linear compressor is 54% while the crank-drive compressor gives 45%. These results indicate that the linear compressor performs better than the conventional crank-drive compressor.

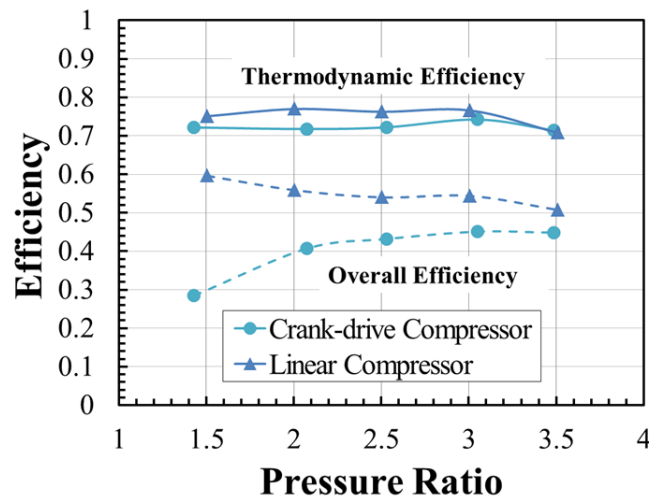


**Fig. 14** Thermodynamic efficiency (adiabatic) and overall efficiency (adiabatic) against pressure ratio for the two compressors; the linear compressor was operated with a 13 mm stroke

To compare the performance of the two compressors running at a fixed pressure ratio, the suction pressure in the crank-drive compressor was manually changed to give a range of mass flow rates, comparable with the mass flow rates with the changing stroke in the linear compressor. Fig. 15 shows the power input for both compressors against the mass flow rate at a pressure ratio of 3.0. The power input increases as the mass flow rate rises, following a similar trend for both compressors. The crank-drive compressor consumes 35 W more electrical power than the linear compressor on average.

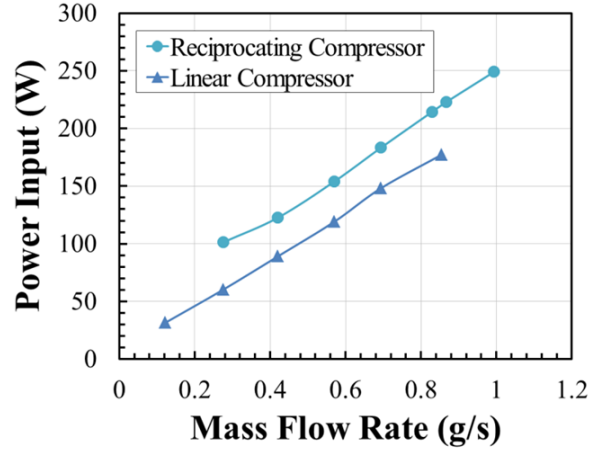


**Fig. 15** Power input for the two compressors as a function of mass flow rate at a pressure ratio of 3.0

## 5.2 Volumetric Efficiency

In a conventional crank-drive compressor, the piston displacement is well defined by the crank mechanism so that clearance volumes approaching zero can be achieved, and this is one of the main advantages of crank-driven compressors. Due to the pressure difference between the cylinder pressure and the compressor body pressure in the linear compressor, the piston will be driven towards the cylinder head (this is known as the ‘DC Offset’ effect). As a result of only indirect control of the piston motion, an appropriate clearance volume is needed to ensure that the piston does not hit the cylinder head during operation.

The theoretical volumetric efficiency is given by:

$$\eta_V = 1 - CL \left[ \left( \frac{P_{dis}}{P_{suc}} \right)^{\frac{1}{n}} - 1 \right] \quad (10)$$

where  $CL$  is the clearance defined as the ratio of the clearance volume to the swept volume.

The actual mass flow was further limited by heat transfer during the suction process, the imperfect nature of the valves, as well as wall friction, leakage and other frictional losses. For the design point of the linear compressor (a pressure ratio of 3.0 and a stroke of 13 mm), the seal leakage is about 14% of the system mass flow rate. Fig. 16 compares the experimental and theoretical volumetric efficiencies for both compressors as a function of the pressure ratio. The linear compressors were operated at the allowable maximum stroke (13 mm) to give the maximum volumetric efficiency for each pressure ratio. The clearance is 2% in the crank-drive compressor and 9% in the linear compressor. This corresponds to a clearance volume of 331 mm<sup>3</sup>, and with a reduction of stroke then the clearance volume increases, for example a stroke of 7 mm gives a clearance volume of 1182 mm<sup>3</sup>. As expected from Equation 10, the volumetric efficiencies in both compressors show a decreasing trend as the pressure ratio is increased. The linear compressor has a lower volumetric efficiency (20% lower on average) than the crank-drive one due to the larger clearance volume and leakage.

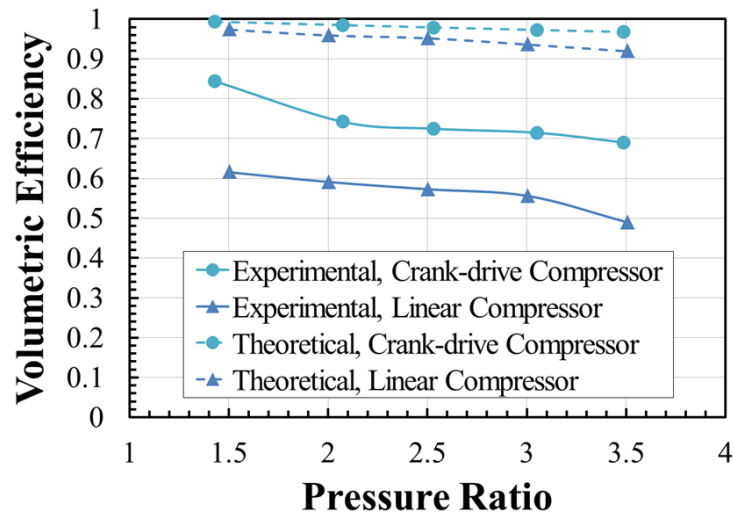


**Fig. 16** Experimental and theoretical volumetric efficiency for the two compressors; the linear compressor was operated with a 13 mm stroke

## 6. Conclusion

Experiments have been conducted to compare a commercial crank-drive compressor and a prototype moving magnet linear compressor. The results demonstrate that the linear compressor generally performs better than the crank-drive compressor, in terms of electrical, mechanical and overall efficiencies.

- (1) The linear motor has a higher efficiency than the rotary induction motor, particularly at low electrical power inputs. The induction motor efficiency increases with the power input.
- (2) The linear motor could reach a higher efficiency (approximately 86% for the design point) with a revised structure to reduce the additional eddy current loss, while the maximum rotary motor efficiency is only about 60%.
- (3) Elimination of the crank and bearings gives a reduction in the mechanical friction losses, which is one of the main benefits of the linear compressor.
- (4) Although the specific losses (e.g. heat transfer, pressure drop, mechanical friction) are not quantified, the mechanical efficiency and adiabatic efficiency provide the key information for both compressors. As the mechanical frictional losses are small and can be assumed to be comparable, it can be argued that the pressure drop losses in the two compressors are very similar.
- (5) The overall adiabatic efficiency is within a range of 52%-60% for the linear compressor, and 28%-45% for the crank-drive compressor.
- (6) The volumetric efficiencies in the crank-drive compressor are much higher than the linear compressor, which is one of the main advantages of the conventional crank-drive compressor with its small clearance volume.

## 7. Acknowledgement

The authors would like to thank the EPSRC for their financial support throughout the construction of the linear compressor (Grant Ref EP/E036899/1).

## 8. References

Bailey, P.B., Dadd, M.W., and Stone, C.R., 2009. An oil-free linear compressor for use with compact



- heat exchangers. In: Proceedings of International Conference on Compressors and their Systems, Institute of Mechanical Engineering, London, pp. 259-268.
- Bailey, P.B., Dadd, M.W., and Stone, C.R., 2010-2011. Cool and straight: linear compressors for refrigeration. In: Proc. Inst. Refrigeration, 4-1.
- Bailey, P.B., Dadd, M.W., Hill, N., Cheuk, C.F., Raab, J., and Tward, E., 2001. High performance flight cryocooler compressor. In: Cryocoolers 11, Kluwer Academic/Plenum Press, New York, pp. 169-174.
- Bansal, P., Vineyard, E., and Abdelaziz, O., 2011. Advances in household appliances – a review. Applied Thermal Engineering, 31, pp. 3748-3760.
- Beale, W. T., and Scheck, C. G., 1986. Electromechanical transducer particularly suitable for a linear alternator driven by a free-piston Stirling Engine. US Patent, 4623808.
- Bradshaw, C.R., Groll, E.A., and Garimella, S.V., 2011. A comprehensive model of miniature-scale linear compressor for electronics cooling. Int. J. Refrigeration, 34, pp. 63-73.
- Bradshaw, C.R., Groll, E.A., and Garimella, S.V., 2012. Linear compressors for electronics cooling: energy recovery and the useful benefits. In: Proceedings of International Compressor Engineering Conference, Purdue, 1134, pp. 1-10.
- Bradshaw, T.W., Delderfield, J., Werret, S.T., and Davey, G., 1986. Performance of the Oxford miniature Stirling cycle refrigerator. Advances in Cryogenic Engineering, Plenum, 31, pp. 801-809.
- Davey, G., 1990. Review of the Oxford cryocooler. Advances in Cryogenic Engineering, Plenum, 35 B, pp. 1423-1430.
- Davies, G.F., Eames, I.W., Bailey, P.B., Dadd, M.W., Janiszewski, A., Stone, C.R., Maidment, G.G., and Agnew, B., 2010. Cooling microprocessors using vapour compression refrigeration. In: Thermal and Thermomechanical Phenomena in Electronics Systems (ITherm), 12<sup>th</sup> IEEE Intersociety Conference, Las Vegas, pp. 1-8.
- Ku, B., Park, J., Hwang, Y., and Lee, J., 2010. Performance evaluation of the energy efficiency of crank-driven compressor and linear compressor for a household refrigerator. In: Proceedings of International Compressor Engineering Conference, Purdue, 1218, pp. 1-8.
- Liang, K., Dadd, M.W., and Bailey, P.B., 2013. Clearance seal compressors with linear motor drive – part i: background and system analysis. Proc. IMechE, Part A: J of Power and Energy, 227(3), pp. 242-251.
- Lilie, D. E. B., 2008 Reciprocating Compressor Driven by a Linear Motor. US Patent, No. 7316547 B2.
- Nasar, S. A., and Boldea, I., 1997. Linear electrodynamic machine and method of making and using same. US Patent, 5654596.
- Yarr, G. A., and Corey, J. A., 1995. Linear electrodynamic machine. US Patent, 5389844.